

Spin-Wave Instabilities and Noncollinear Magnetic Phases of a Geometrically Frustrated Triangular-Lattice Antiferromagnet

J. T. Haraldsen,¹ M. Swanson,^{1,2} G. Alvarez,³ and R. S. Fishman¹

¹Materials Science and Technology Division, Oak Ridge National Laboratory, Oak Ridge, Tennessee 37831, USA

²Department of Physics, North Dakota State University, Fargo, North Dakota 58105, USA

³Computer Science & Mathematics Division and Center for Nanophase Materials Sciences, Oak Ridge National Laboratory, Oak Ridge, Tennessee 37831, USA

(Received 15 January 2009; published 12 June 2009)

This Letter examines the relation between the spin-wave instabilities of collinear magnetic phases and the resulting noncollinear phases for a geometrically frustrated triangular-lattice antiferromagnet in the high-spin limit. Using a combination of phenomenological and Monte Carlo techniques, we demonstrate that the instability wave vector with the strongest intensity in the collinear phase determines the wave vector of a cycloid or the dominant elastic peak of a more complex noncollinear phase. Our results are related to the observed multiferroic phase of Al-doped CuFeO₂.

DOI: 10.1103/PhysRevLett.102.237204

PACS numbers: 75.30.Ds, 75.50.Ee, 61.05.fg

It is well known that the transition between different magnetic ground states may be signaled by the softening of a spin-wave (SW) mode [1]. In the simplest case of a conventional square-lattice antiferromagnet, the softening of a SW mode at wave vectors $(\pi, 0)$ and $(0, \pi)$ signals the spin flop and canting of the magnetic moments at a critical field. In the manganites [2], the SW instabilities of the ferromagnetic state have been used to construct the phase diagram for the antiferromagnetic (AFM) phases that appear with Sr doping. The softening of a SW excitation at $(\pi, 0)$ signals the instability of the Néel state and the canting of the spins in a spin-1/2 union-jack lattice [3]. But the relation between the SW instabilities of a collinear phase and a resulting noncollinear phase is less clear when multiple SW instabilities occur simultaneously or when the noncollinear phase has a complex magnetic structure with several elastic peaks. This Letter explores the relation between the SW instabilities of the collinear 4 and 8-sublattice (SL) phases of a geometrically frustrated triangular-lattice antiferromagnet (TLA) and the noncollinear phases that appear with decreasing anisotropy D . We show that when multiple SW instabilities of the collinear phase occur at once, the instability wave vector with the largest intensity determines the dominant ordering wave vector of the resulting noncollinear phase [4]. One of the predicted noncollinear phases may be related to the multiferroic phase that appears in CuFeO₂ with Al doping [5].

Frustrated TLAs with AFM nearest-neighbor exchange $J_1 < 0$ exhibit a remarkable number of competing ground states [6]. With interactions J_i up to third nearest neighbors (denoted in Fig. 1) and assuming Ising spins along the z direction, Takagi and Mekata [7] obtained a phase diagram with ferromagnetic (FM), 2-SL, 3-SL, 4-SL, and 8-SL phases. A portion of that phase diagram is sketched in Fig. 1. For the geometrically frustrated TLA CuFeO₂ in

fields below 7 T, the ground state is the 4-SL phase [8,9] and the black dot in Fig. 1 denotes the estimated ratio of exchange parameters $J_2/|J_1| \approx -0.44$ and $J_3/|J_1| \approx -0.57$ [10,11].

As demonstrated by the small SW gap of about 0.9 meV [5,10] on either side of the ordering wave vector $\mathbf{q} = \pi\mathbf{x}$, the spin fluctuations of CuFeO₂ are much softer than would be expected for Ising spins. With Heisenberg spins, the collinear magnetic phases of a TLA become locally unstable below a critical anisotropy D_c that depends on the exchange parameters J_i . The observed softening of the SW modes in CuFe_{1-x}Al_xO₂ with Al doping [5] can be reproduced by lowering D towards D_c [12] in the 4-SL I region of Fig. 1. For Al concentrations above about $x_c \approx 0.016$,

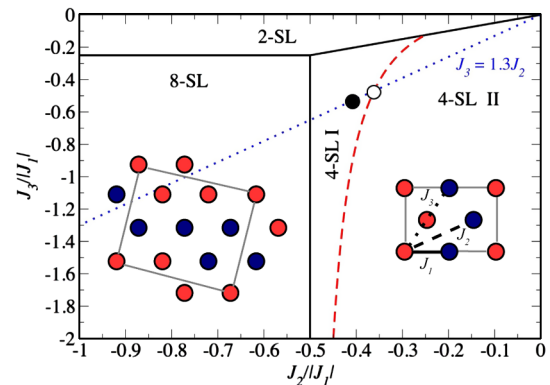


FIG. 1 (color online). A portion of the TLA phase diagram for large D and $J_1 < 0$. The dashed (red) curve divides the 4-SL phase into 4-SL I and 4-SL II regions. For the 4 and 8-SL phases, light red circles denote up spins and dark blue circles denote down spins; the solid (gray) line defines the unit cell. The dashed (blue) line obeys the relation $J_3 = 1.3J_2$, the black circle is the estimated location of the exchange parameters for CuFeO₂, and the white circle lies on the boundary between the 4-SL I and 4-SL II regions.

the magnetic ground state of $\text{CuFe}_{1-x}\text{Al}_x\text{O}_2$ becomes noncollinear and displays multiferroic properties [13–15].

We have determined the ground-state magnetic phases of the TLA using a combination of Monte Carlo (MC) simulations and phenomenological techniques. The TLA Hamiltonian is

$$H = -\frac{1}{2} \sum_{i \neq j} J_{ij} \mathbf{S}_i \cdot \mathbf{S}_j - D \sum_i S_{iz}^2, \quad (1)$$

where J_{ij} includes first, second, and third-neighbor interactions (shown in Fig. 1). The nearest-neighbor distance has been set to 1. The SW frequencies $\omega_{\mathbf{k}}^{(t)}$ of the collinear phases are obtained by performing a Holstein-Primakoff $1/S$ expansion about the classical limit. The SW intensities $W_{\mathbf{k}}^{(t)}$ are the prefactors in the spin-spin correlation function $S(\mathbf{k}, \omega) = \sum_t W_{\mathbf{k}}^{(t)} \delta(\omega - \omega_{\mathbf{k}}^{(t)})$ [16]. The intensities $W_{\mathbf{k}}^{(t)}$ correspond to the strength of the spin fluctuations associated with the wave vector \mathbf{k} and SW branch t . Above the critical anisotropy D_c , a collinear phase is locally stable if the SW frequencies are positive and real for every wave vector.

MC simulations were used to find the noncollinear magnetic phases of the TLA. The simulations were started at a temperature high enough to rule out metastable states. To mimic the process of thermal annealing, the system was slowly cooled to a final temperature (in units of $|J_1|S^2$) ranging from 4×10^{-3} to 1×10^{-4} . Lowering the final temperature further did not significantly change the resulting noncollinear phase. Using lattices of varying sizes with periodic boundary conditions, we found that there was no substantial change for lattices greater than 16×16 .

In Fig. 1, the 4-SL phase is separated into regions I and II by the curve $J_1/J_2 - 2 = J_2/J_3$. In region 4-SL II, the instability wave vectors are given by $\mathbf{k} = (\pi \pm \pi/3)\mathbf{x}$, independent of the exchange parameters; in region 4-SL I, the instability wave vectors depend on the exchange parameters [4]. With the exchange parameters corresponding to the black circle in region 4-SL I, we determined the stable magnetic phases as a function of D . As shown in Fig. 2, the 4-SL phase is stable down to $D/|J_1| \approx 0.27$, below which MC simulations obtain the complex noncollinear (CNC) phase shown on the top of Fig. 2. While the CNC phase is translationally invariant in the y direction, it retains some of the FM correlations present in the 4-SL phase: the same up or down spin frequently occurs at sites $\mathbf{R} = m\mathbf{x} + n\sqrt{3}\mathbf{y}$ and $\mathbf{R}' = \mathbf{R} + \mathbf{x}/2 + \sqrt{3}\mathbf{y}/2$ or $\mathbf{R}'' = \mathbf{R} - \mathbf{x}/2 + \sqrt{3}\mathbf{y}/2$. Although the MC boundary conditions prevent a definitive determination, the CNC phase is probably incommensurate in the x direction.

Below a second threshold value of $D/|J_1| \approx 0.08$, a cycloid like the one sketched in the bottom panel of Fig. 2 [17] has a lower energy than the CNC phase. As discussed below, the wave vector of the cycloid is inde-

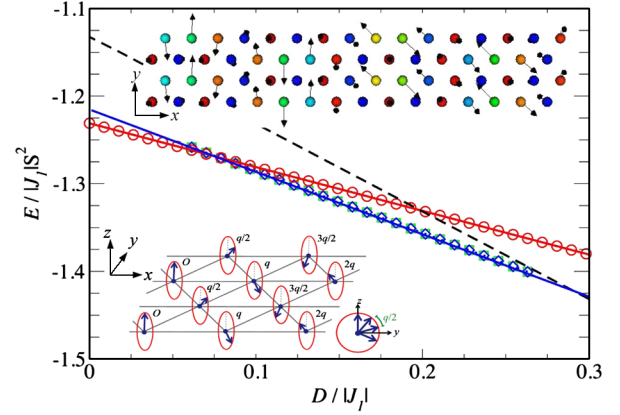


FIG. 2 (color online). Energy as a function of $D/|J_1|$ for the 4-SL (black dashed), CNC (blue diamonds), and cycloid I (red circles) phases with $J_3/J_2 = 1.3$ and $J_1/J_2 = 2.28$. The bottom diagram shows the cycloid for arbitrary q . The top diagram shows the CNC phase, where local moments range from red (purely up, $+\mathbf{z}$) to blue (purely down, $-\mathbf{z}$) and arrows indicate moment direction.

pendent of D . If the CNC phase were removed, then the cycloid would achieve a lower energy than the 4-SL phase below $D/|J_1| \approx 0.2$, still above the critical value $D_c/|J_1| \approx 0.15$ for the local stability of the 4-SL phase. The cycloid energy in Fig. 2 was obtained numerically with the cycloid restricted by finite boundary conditions.

To gain a better understanding of the phases stabilized within the TLA, we have evaluated the magnetic phases along the line with $J_3/J_2 = 1.3$ drawn through the black

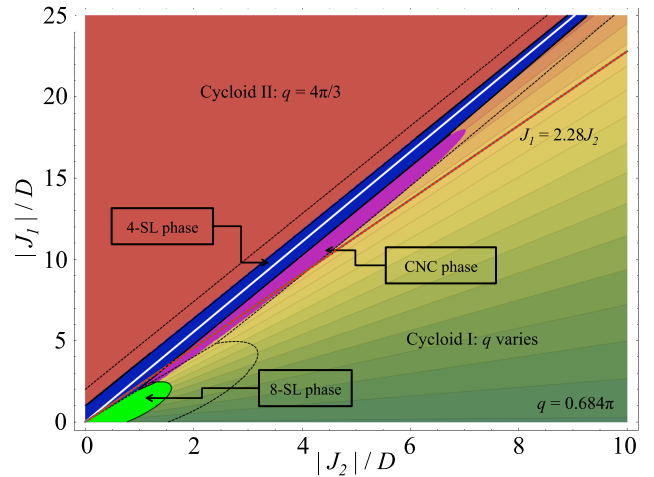


FIG. 3 (color online). Phase diagram for the TLA as a function of $|J_1|/D$ and $|J_2|/D$ with $J_3 = 1.3J_2$ containing five regions: 4-SL (dark blue), 8-SL (light green), CNC (light violet), cycloid I (variable green-orange), and cycloid II (solid red). The dashed (white) line separates regions 4-SL I and 4-SL II. The dotted (black) curves denote the metastable boundaries for the 4-SL and 8-SL regions. Cycloid I has wave vectors q that range from 0.684π to 0.923π in intervals of 0.016π .

dot in Fig. 1. Five stable phases are presented as a function of $|J_1|/D$ and $|J_2|/D$ in Fig. 3. The 4-SL phase is stable along a strip through the diagonal of this plot. Although not indicated by this figure, the 4-SL region disappears above $|J_1|/D \approx 40$. Close to the origin or for large D , a collinear 8-SL region is indicated in Fig. 1. Two cycloids are also obtained: in the upper left, cycloid II with wave vector $4\pi\mathbf{x}/3$; in the lower right, cycloid I with the variable wave vector indicated in the figure [17]. Finally, a CNC phase appears just below the 4-SL phase and disappears above $|J_1|/D \approx 20$. Regions of local stability for the collinear phases are indicated in Fig. 3 by the dashed black curves [4]. The results in Fig. 2 can be obtained from Fig. 3 by drawing a line from the origin with slope 2.28 (dashed red or gray) (so that $J_2/|J_1| = -0.44$), which passes from the 4-SL phase through the CNC phase into cycloid I.

The classical energies of each of these phases can be written as $E/NS^2 = A_1J_1 + A_2J_2 + A_3J_3 - A_D D$, with coefficients given in Table I. Only a noncollinear phase with $0.5 < A_D < 1$ can intercede between a collinear phase with $A_D = 1$ and a cycloid with $A_D = 0.5$. For the CNC phase with $A_D \approx 0.71$, the error bars indicate the range of parameters obtained from MC simulations near $|J_1|/D = 5.7$ and $|J_2|/D = 2.5$. Using the resulting MC spin configurations, the CNC energy is close to a linear function of the exchange interactions and anisotropy, allowing us to obtain the phase space in Fig. 3. Table I indicates that the CNC phase is characterized by rather weak next-neighbor correlations with small $|A_2|$.

The stability of cycloids I and II in Fig. 3 have been confirmed using MC simulations. The ordering wave vector $\mathbf{q} = q\mathbf{x}$ of cycloid I is evaluated by minimizing E with respect to q , where q depends only on the ratios J_2/J_1 and J_3/J_2 , as indicated by the diagonal lines in Fig. 3. Cycloid II with $q = 4\pi/3$ corresponds to the 120° Néel state found in a classical TLA with $D = 0$ and $J_3 = 0$ [18]. Although slightly distorted, the Néel state remains stable for nonzero D over the range of exchange parameters in Fig. 3.

With decreasing D or moving away from the origin of Fig. 3 along a diagonal, the 4-SL phase becomes unstable either to cycloid II or to the CNC phase. The white line bisecting the 4-SL region in Fig. 3 corresponds to the white point in Fig. 1 at the border between the 4-SL I and 4-SL II regions with $J_2/|J_1| = -0.36$. In region 4-SL II or above the white diagonal line, the 4-SL phase has instabilities at

the wave vectors $(\pi \pm \pi/3)\mathbf{x}$. The SW intensity at the larger of these two wave vectors always dominates and the 4-SL phase evolves into cycloid II with wave vector $4\pi\mathbf{x}/3$.

In region 4-SL I, the 4-SL phase has three unique SW instabilities: one at wave vector \mathbf{k}_1 along the \mathbf{x} axis, another at \mathbf{k}_2 rotated by $\pi/3$, and a third at \mathbf{k}_3 rotated by $-\pi/3$. All three have the same magnitude with $\pi/2 < k_i < \pi$. Other SW instabilities in the 4-SL I region can be related by a symmetry operation to one of these three. We find that the instability at \mathbf{k}_1 always has a larger intensity than the “twins” at \mathbf{k}_2 or \mathbf{k}_3 or than any of the other wave vectors related by symmetry. Correspondingly, cycloid I along any diagonal in Fig. 3 has the same wave vector \mathbf{q} as the dominant instability of the 4-SL phase.

Similar conclusions are reached for the 8-SL phase, which switches to cycloid I along any diagonal in Fig. 3. Although the SW instability of the 8-SL phase occurs simultaneously at several wave vectors, the dominant wave-vector instability of the 8-SL phase coincides with the wave vector \mathbf{q} of cycloid I along any diagonal in Fig. 3.

However, the CNC phase that intercedes between the 4-SL and cycloid I phases is characterized by several elastic peaks shown in Fig. 4(c). Within the precision of our MC simulations, the dominant wave vector $\mathbf{k} \approx 0.87\pi\mathbf{x}$ of the CNC phase coincides with the dominant instability wave vector of the 4-SL phase that precedes it.

To demonstrate how the magnetic ground state evolves from cycloid II into the 4-SL phase and then into cycloid I, we plot in Figs. 4(a) and 4(b) the SW frequencies and intensities versus wave vector for the 4-SL phase with $J_1/D = -5.5$, $J_3/J_2 = 1.3$, and $|J_2|/D$ varying from 1.30 to 2.67. As $|J_2|/D$ approaches the lower limit for the stability of the 4-SL phase, the SW intensity dominates at the cycloid II wave vector $\mathbf{q} = 4\pi\mathbf{x}/3$. At the upper limit, the cycloid I wave vector $\mathbf{q} \approx 0.83\pi\mathbf{x}$ dominates. We concluded that the wave vectors of the SW instabilities for the collinear phases correspond to the ordering wave vectors of the noncollinear phases.

The CNC phase may be related to the multiferroic phase observed in Al-doped CuFeO_2 [5], which was recently investigated by Nakajima *et al.* [19]. Based on neutron-scattering measurements, those authors concluded that the ground state is a modified cycloid with the same spin on sites \mathbf{R} and \mathbf{R}' (see above). This phase has peaks at

TABLE I. Energy coefficients for collinear, cycloid, and CNC phases.

Phase	A_1	A_2	A_3	A_D
4-SL	1	-1	1	1
8-SL	0	1	1	1
Cycloid I	$-(\cos(q) + 2\cos(q/2))$	$-(1 + 2\cos(3q/2))$	$-(\cos(2q) + 2\cos(q))$	1/2
Cycloid II	3/2	-3	3/2	1/2
CNC	0.595 ± 0.001	-0.097 ± 0.001	1.159 ± 0.001	0.712 ± 0.001

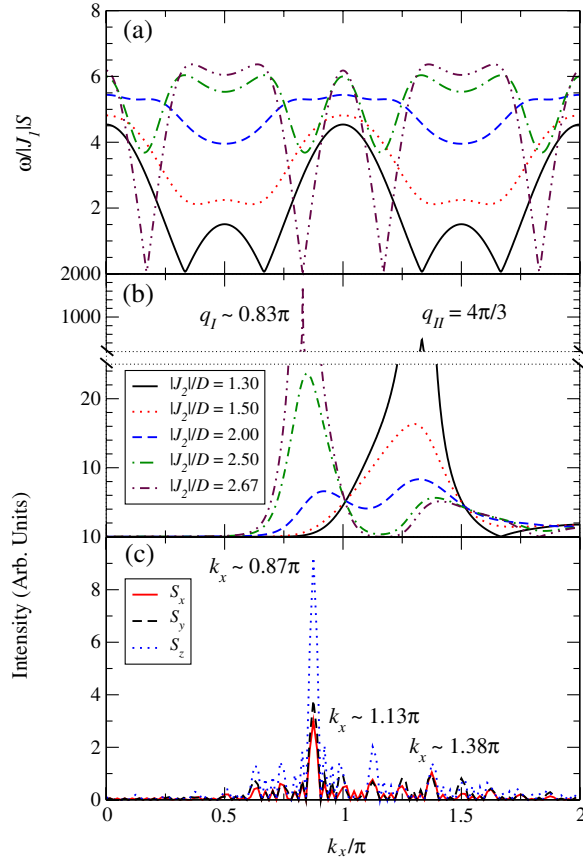


FIG. 4 (color online). (a),(b) SW frequency and intensity versus wave vector k_x for the 4-SL phase with $|J_1|/D = 5.5$, $J_3 = 1.3J_2$, where $|J_2|/D$ varies from 1.30 to 2.67. (c) Fourier transform for the S_x , S_y , and S_z components of the CNC phase with the same exchange parameters as above and $|J_2|/D = 2.5$.

wave vectors on either side of $\pi\mathbf{x}$, in agreement with the neutron measurements. However, a modified cycloid cannot be stabilized by a Hamiltonian with the form of Eq. (1), regardless of the exchange and anisotropy parameters. With an additional phase slip δ for the spins at sites \mathbf{R}' , a pure cycloid with $\delta = 0$ and a single elastic peak always has lower energy than the phase proposed in Ref. [19] with $\delta = -q/2$. This conclusion has been verified by MC simulations.

Like the noncollinear phase proposed earlier [19], the CNC phase also contains FM correlations between sites \mathbf{R} and \mathbf{R}' or \mathbf{R}'' . So the CNC phase also has elastic peaks on either side of $\pi\mathbf{x}$ at $k_x \approx 0.87\pi$ and 1.13π , as shown in Fig. 4(c). Because the FM correlations are not perfect and vary along the \mathbf{x} direction, the CNC phase contains several other elastic peaks that may allow it to be experimentally distinguished from the phase proposed in Ref. [19].

To summarize, we demonstrate for the first time that the dominant ordering wave vector of a noncollinear phase corresponds to the dominant instability wave vector of

the preceding collinear phase. Thus, complex noncollinear phases can be more easily characterized by studying the SW instabilities of collinear phases with stronger anisotropy. While the connection between the SW instabilities and the dominant wave vector of the noncollinear phases was demonstrated numerically for a frustrated TLA, we hope to establish that connection more generally in future work. We also argue that the CNC phase sketched in Fig. 2 is a more reasonable candidate for the multiferroic phase observed in Al-doped CuFeO_2 than the one previously proposed.

This research was sponsored by the Laboratory Directed Research and Development Program of Oak Ridge National Laboratory, managed by UT-Battelle, LLC for the U.S. Department of Energy under Contract No. DE-AC05-00OR22725 and by the Division of Materials Science and Engineering and the Division of Scientific User Facilities of the U.S. DOE.

- [1] R.M. White, *Quantum Theory of Magnetism* (Springer, Berlin, 2007).
- [2] Z. Fang, I. V. Solov'yev, and K. Terakura, Phys. Rev. Lett. **84**, 3169 (2000).
- [3] W. Zheng, J. Oitmaa, and C.J. Hamer, Phys. Rev. B **75**, 184418 (2007).
- [4] M. Swanson, J.T. Haraldsen, and R.S. Fishman, Phys. Rev. B **79**, 184413 (2009).
- [5] N. Terada *et al.*, J. Magn. Magn. Mater. **272–276**, e997 (2004); Phys. Rev. B **70**, 174412 (2004); J. Phys. Condens. Matter **19**, 145241 (2007).
- [6] See, for example, *Frustrated Spin Systems*, edited by H. T. Diep (World Scientific, New Jersey, 2004).
- [7] T. Takagi and M. Mekata, J. Phys. Soc. Jpn. **64**, 4609 (1995).
- [8] S. Mitsuda *et al.*, J. Phys. Soc. Jpn. **60**, 1885 (1991).
- [9] M. Mekata *et al.*, J. Phys. Soc. Jpn. **62**, 4474 (1993).
- [10] F. Ye *et al.*, Phys. Rev. Lett. **99**, 157201 (2007).
- [11] R. S. Fishman *et al.*, Phys. Rev. B **78**, 140407(R) (2008).
- [12] R. S. Fishman, J. Appl. Phys. **103**, 07B109 (2008).
- [13] T. Kimura, J. C. Lashley, and A. P. Ramirez, Phys. Rev. B **73**, 220401(R) (2006).
- [14] S. Kanetsuki *et al.*, J. Phys. Condens. Matter **19**, 145244 (2007).
- [15] S. Seki *et al.*, Phys. Rev. B **75**, 100403(R) (2007).
- [16] G.L. Squires, *Introduction to the Theory of Thermal Neutron Scattering* (Dover, New York, 1996).
- [17] Because of the anisotropy, the cycloids will be slightly distorted by the tilting of the spins towards the $\pm z$ directions with an energy gain of order $D^2 S^2 / z |J_1|$ ($z = 6$ is the number of nearest neighbors). Within the precision of our MC simulations, this distortion is undetectable and a pure cycloid is obtained.
- [18] Th. Jolicoeur *et al.*, Phys. Rev. B **42**, 4800 (1990).
- [19] T. Nakajima *et al.*, J. Phys. Soc. Jpn. **76**, 047309 (2007).